Prepublished copy

Nature Environment & Pollution Technology

This is a peer-reviewed prepublished version of the paper to be published in Vol. 25, No. 2, June 2026 issue

Original Research

Integrating Real-Time Monitoring and 3D Hydrodynamic Modeling to Assess Tidal Impacts on Water Quality in a Mangrove-Influenced Aquaculture Zone in Central Sulawesi, Indonesia

Pasjan Satrimafitrah[1]†, Sabhan Sabhan[2], Moh. Iqbal[3], Nov Irmawati Inda[1] and Aiyen Tjoa[4]

[1]Department of Chemistry, Faculty of Mathematics and Natural Sciences, Tadulako University, Indonesia

[2]Department of Physics, Faculty of Mathematics and Natural Sciences, Tadulako University, Indonesia

[3]Department of Biology, Faculty of Mathematics and Natural Sciences, Tadulako University, Indonesia

[4]Department of Agrotechnology, Faculty of Agriculture, Tadulako University, Indonesia

†Corresponding author: Pasjan Satrimafitrah; pasjan@untad.ac.id

Pasjan Satrimafitrah (https://orcid.org/0000-0003-3317-8086), Sabhan Sabhan (https://orcid.org/0000-0001-9105-4175), Moh. Iqbal (https://orcid.org/0000-0002-2601-5185), Nov Irmawati Inda (https://orcid.org/0000-0002-9866-239X), Aiyen Tjoa (https://orcid.org/0000-0003-0583-9174)

Key Words	Tidal dynamics, Water quality monitoring, Mangrove ecosystem, Aquaculture management, Real-time sensors
DOI	https://doi.org/10.46488/NEPT.2026.v25i02.D1857 (DOI will be active only after the final publication of the paper)
Citation for the Paper	Satrimafitrah, P., Sabhan, S., Iqbal, M., Inda, N.I. and Tjoa, A., 2026. Integrating real-time monitoring and 3D hydrodynamic modeling to assess tidal impacts on water quality in a mangrove-influenced aquaculture zone in central Sulawesi, Indonesia. *Nature Environment and Pollution Technology*, 25(2), D1857. https://doi.org/10.46488/NEPT.2026.v25i02.D1857

ABSTRACT

(1) Background: Understanding how tidal fluctuations affect water quality in estuarine and mangrove-influenced aquaculture zones is essential for healthy and productive ponds. This study investigated how key water quality parameters respond to tidal changes in the Tanah Mea estuary, Central Sulawesi, Indonesia. (2) Methods: A PC-based real-time Water Quality Monitoring System (WQMS) and IoT sensors were deployed in situ to record high-frequency data, while Open-Flows Flood software was used to simulate the spatial distribution of temperature, salinity, nitrite, and dissolved oxygen (DO) during the tidal cycles. Correlation analyses (Pearson and Spearman, corrected for autocorrelation) were employed to quantify the relationship between water level and each measured parameter. (3) Results: Continuous monitoring from March to April 2025 yielded 9,537 valid observations. The results showed strong inverse correlations between tidal height and both pH and DO, with weaker relationships for nitrite, temperature, and salinity, while EC exhibited minimal correlation with tides. Spatial simulations indicated clear gradients of DO and salinity from upstream to open waters, with dilution and oxygenation improving further

from the estuary. However, DO values from WQMS did not fully align with modern patterns. (4) Conclusion: Tidal dynamics play a key role in shaping estuarine water quality. Integrating real-time monitoring and 3D modelling provides complementary insights and supports practical recommendations for sustainable aquaculture, specifically scheduling pond water intake shortly after low tide to maximize DO and minimize nitrite levels.

INTRODUCTION

Mangrove ecosystems in Indonesia are among the most diverse and extensive in the world, playing a crucial role in supporting both marine and terrestrial biodiversity (Rahman *et al.*, 2024). It helps maintain the ecological balance of the coast by protecting shorelines from storms like tsunamis, stabilizing sediments, and supporting nutrient cycles. It also acts as a biological filter by trapping sediments and absorbing pollutants from land-based waste (Lam *et al.*, 2023). Tidal dynamics significantly influence the mangrove ecosystem by regulating the distribution of nutrients, sediment movement, and salinity, which are essential for ecological balance and supporting the growth of mangroves. Studies have shown that an increase in rainfall and terrestrial runoff may lower salinity levels, which ultimately enhance the growth and productivity of certain mangrove species (Singh, Thirumurugan, and Prabakaran, 2024). Conversely, reduction of rainfall may lead to increased salinity, which potentially results in decreased productivity and shifts in the composition of species due to intensified competition (Singh, 2020). This highlights the vital role of the tidal zone in maintaining the ecological stability of mangrove ecosystems.

Several studies have reported a strong correlation between mangrove density and water quality indices. Areas with a higher density of mangrove tend to exhibit improved water conditions, which in turn promotes the presence of aquatic organisms, such as plankton, a key component of the food web's ecosystem (Palit *et al.*, 2022). Moreover, mangrove habitats provide important breeding and nursery grounds for various marine species, thereby contributing to the sustainability of fisheries and enhancing coastal biodiversity (Suharno and Saraswati, 2020).

The transformation of land surrounding mangroves into shrimp ponds has a direct impact on water quality. Mangroves normally filter sediments and excessive nutrients, but their removal leads to runoff and pollution, degrading coastal waters and increasing the risk of eutrophication (Kusumaningtyas *et al.*, 2022; Mitra and Sikder, 2023). Water quality needs to be analyzed frequently to ensure optimal environmental conditions for aquatic life, prevent risks related to pollution, and support sustainable aquaculture practices. Traditional approaches to measuring water quality involve manual sampling techniques, which often rely on laboratory analyses. Despite their historical significance, these approaches have a number of drawbacks. For example, they are time-consuming, labor-intensive, and prone to human error, which could result in inaccurate data collection and insufficient coverage of water quality conditions in terms of time or space (Srivastava, Vaddadi and Sadistap, 2018; Wang *et al.*, 2018). Reliance on manual techniques can frequently impede timely reactions to pollution incidents because samples must be gathered, transported, and examined in a laboratory (Guo *et al.*, 2020).

In order to ensure water sourced from the mangrove area remains stable for aquaculture, a reliable water quality measurement is required, particularly in a real-time monitoring system. It changes how water management works by using cutting-edge technology like the Internet of Things (IoT) and various sensor types to measure parameters like turbidity, pH, temperature, and chemical concentrations continuously and instantaneously (Essamlali, Nhaila and El Khaili, 2024; Singh and Walingo, 2024; Abdelmoneim *et al.*, 2025). This system not only provides immediate insights into water quality but also enables proactive strategies.

This study addresses the question, "How do tidal fluctuations regulate key water quality parameters in mangrove estuaries, and what are the implications for aquaculture water intake management?". To answer this challenge, we explore how tidal changes affect water quality in mangrove areas that supply water to nearby aquaculture or shrimp ponds in Central Sulawesi, Indonesia. By closely monitoring how key water quality parameters, such as salinity, pH, dissolved oxygen, nitrite, and temperature, shift during tidal phases, we aim to better understand when conditions are most suitable for drawing water into the ponds. The goal is to help farmers manage their water more effectively, reduce environmental risks, and support more sustainable aquaculture practices that work in harmony with natural coastal systems.

2. MATERIALS AND METHODS

Study site

This study was conducted in a mangrove estuarine area located in Tanah Mea, Central Sulawesi, Indonesia, which serves as a primary water source for traditional aquaculture ponds in the surrounding region. The site was selected based on its ecological classification as a river-mouth mangrove system with active tidal exchange. The presence of dense mangrove vegetation was confirmed by field verification and satellite imagery. The coordinates of the monitoring station are –0.6873734, 119.7779482, as shown in Fig. 1.

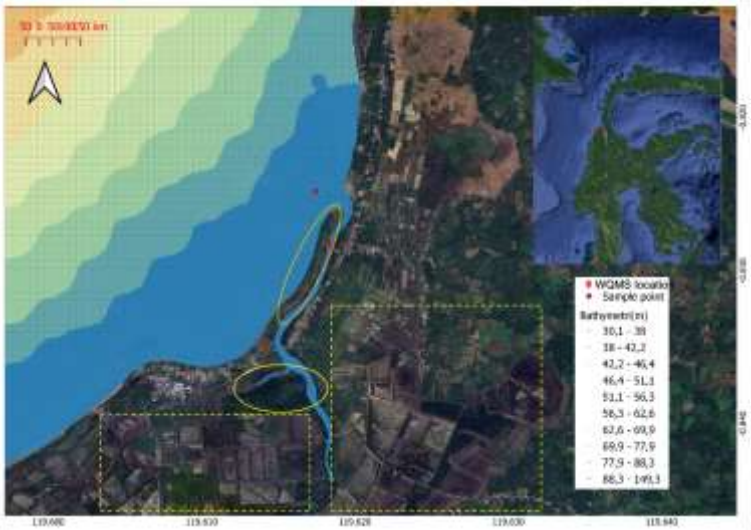

Fig. 1: Bathymetry map for WQMS in mangrove estuary near traditional aquaculture ponds. (Red dot: sample point for 3D hydrodynamic study; red location pin: WQMS location; yellow solid line: mangrove estuarine; yellow dashed line: traditional aquaculture area). The image was generated using QGIS.

Water Quality and Tidal Monitoring

Water quality parameters in this study were measured using WQMS (Water Quality Measuring System) tools, which contain DO, temperature, salinity, and pH sensors, while tidal fluctuations were monitored using a water level sensor (Indosat Ooredoo-PT. Nocola IoT Solution). The collected data were processed using a built-in computational system and recorded every minute onto a flash drive. In order to enable real-time monitoring, the recorded data were transmitted to a website via 4G LTE communication, utilizing a Modbus protocol installed within a dedicated panel box. The entire monitoring system was powered by a solar panel, making it suitable for remote coastal or mangrove locations where conventional grid electricity is not available (Fig. 2).

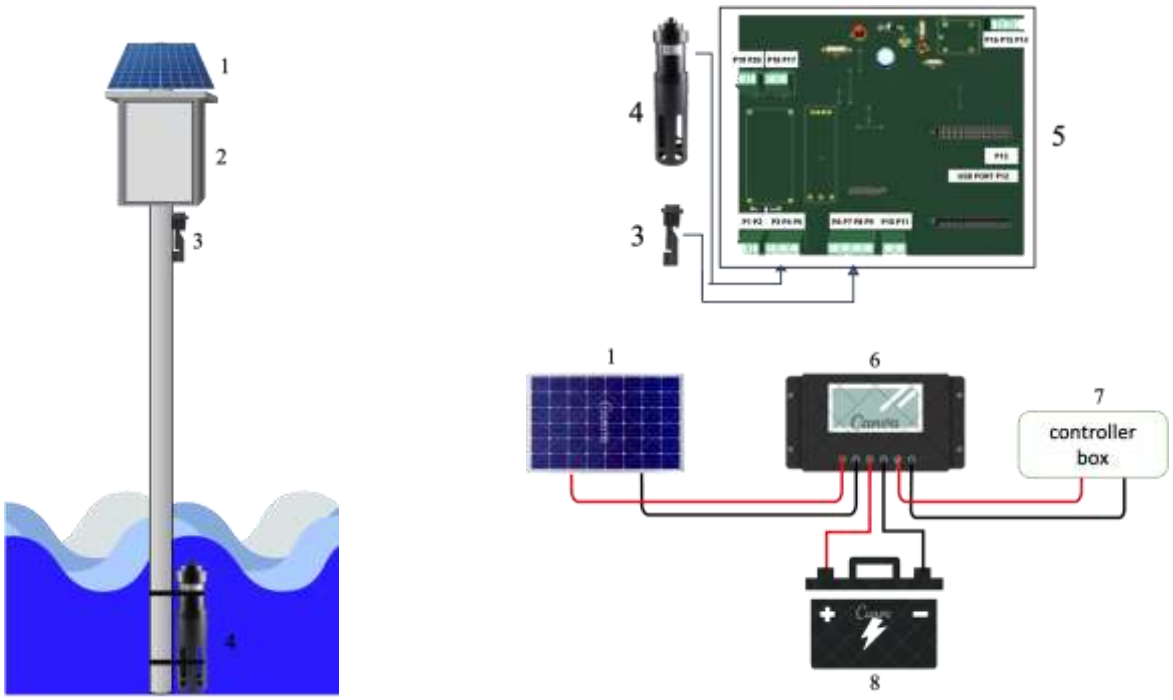

Fig. 2: Schematic diagram of the water quality and tidal monitoring system (1. Solar panel, 2. Panel box, 3. Water level sensor, 4. WQMS sensor, 5. Fluxbox controller, 6. Solar charge controller, 7. Controller box, 8. Battery)

The specifications of the sensors used for measuring water quality and tidal levels are summarized in Table 1.

Table 1: Specifications of sensors used for measuring water quality parameters and water level.

Parameter	DO	Temperature	Salinity	pH	Water Level	Nitrite
Measuring Range	0–20 mg/L	0–50 °C	0–5000 µS/cm	0–14 pH	25–750 cm	0.1-1000 mg/L
Accuracy	±0.4 mg/L	±0.5 °C	±1 µS/cm	±0.1 pH	±(1 cm + S × 0.3%)	± 2.5%
Resolution	0.01 mg/L	0.1 °C	±1.5% F.S.	0.01 pH	—	0.1 mg/L

Energy captured by solar panels was stored in a sealed lead-acid battery housed within the panel box, which ensures uninterrupted operation of the system during nighttime or cloudy/rainy days. The design allows for autonomous, long-term operation in the field with minimal maintenance.

Data collection and statistical analysis

Sensor data were collected at one-minute intervals and exported in .csv format. Prior to analysis, the data were cleaned by removing outliers and missing values through interquartile range-based filtering and manual inspection.

Because monitoring was conducted at 1-minute intervals (N = 9,537 valid observations after quality control), we tested all time-series variables for serial dependence and corrected the correlation analyses accordingly. Lag-1 autocorrelations (r_1) were obtained from the autocorrelation function (ACF) plots for each parameter. For pairwise correlation tests with water level, we estimated the effective sample size (N_eff) (Pyper and Peterman, 1998):

$$N_{eff} = N.\frac{1-r_{1,x}r_{1,y}}{1+r_{1,x}r_{1,y}} \quad (1)$$

where are the lag-1 autocorrelations of the two series, and N is the raw number of observations.

To evaluate the strength and direction of the relationship between tidal height and individual water quality parameters, both Pearson product-moment correlation and Spearman rank correlation analyses were performed using Free Statistics Software by Office for Research, Development and Education (ORDE) (Wessa, 2025).

3D hydrodynamic modelling

The water quality parameter distribution model utilized the biogeochemical module found in OpenFlows Flood (Bentley), employing a volume-based approach with generic vertical discretization using the z-sigma vertical coordination type. The model was built using the Navier-Stokes equations with Boussinesq and hydro-static approaches for the continuity equation, momentum equations as follows:

$$\frac{\partial u}{\partial x}+\frac{\partial v}{\partial y}+\frac{\partial w}{\partial z}=0 \quad \ldots(1)$$

$$\frac{\partial u}{\partial t}+u\frac{\partial u}{\partial x}+v\frac{\partial u}{\partial y}+w\frac{\partial u}{\partial z}-fv=\frac{1}{\rho_0}\frac{\partial p}{\partial x}+\frac{\partial}{\partial x}\left(\nu_H\frac{\partial u}{\partial x}\right)+\frac{\partial}{\partial y}\left(\nu_H\frac{\partial u}{\partial y}\right)+\frac{\partial}{\partial z}\left(\nu_t\frac{\partial u}{\partial z}\right) \quad \ldots(2)$$

$$\frac{\partial v}{\partial t}+u\frac{\partial v}{\partial x}+v\frac{\partial v}{\partial y}+w\frac{\partial v}{\partial z}+fu=\frac{1}{\rho_0}\frac{\partial p}{\partial x}+\frac{\partial}{\partial x}\left(\nu_H\frac{\partial v}{\partial x}\right)+\frac{\partial}{\partial y}\left(\nu_H\frac{\partial v}{\partial y}\right)+\frac{\partial}{\partial z}\left(\nu_t\frac{\partial v}{\partial z}\right) \quad \ldots(3)$$

$$\frac{\partial p}{\partial z}=-\rho.g \quad \ldots(4)$$

where: u, v, and w are the velocities in the x, y, and z directions (m/s), f is the Coriolis parameter (rad/s), ν_H and ν_t are the coefficients of horizontal and vertical turbulent viscosity (m^2/s), p is the pressure (Pa), ρ_0 is the reference density (kg/m^3).

To observe the spatial distribution of water quality parameters, a water quality model was created based on input data obtained from WQMS tools. This model encompasses the river flow and the sea in front of the river mouth, as presented in Error! Reference source not found.. The hydrodynamic model was executed on a horizontal grid with a resolution of 0.0001° × 0.0001° (≈ 11.1 m × 11.1 m). The vertical coordinate system employed a z-sigma framework with a single depth-averaged layer. Turbulence was represented using the Smagorinsky formulation. Boundary forcing consisted of harmonic tidal constituents at the open boundary and river discharge at the upstream boundary. This configuration enables the model to capture horizontal advection and tidal propagation at high spatial resolution; however, being depth-averaged, it does not resolve vertical stratification within the water column. Model outputs compared with WQMS observations correspond to the cell-averaged DO and other variables at the grid node nearest to the sensor location.

Table 2. shows input based on the measurements from the installed WQMS device. The model was generated by tides with tidal constants as shown in Table 3. The upstream boundary of the model represents the riverine inflow characterized by freshwater (salinity ≈ 0.01 PSU), whereas the WQMS station is located near the estuary mouth under strong tidal influence, where observed salinity ranges from 18 to 30 PSU. This natural salinity gradient was reproduced by the model to represent mixing between riverine and marine water masses.

Table 2: River discharge parameters for model input.

No.	Parameter	Value	Unit
1	Discharge	30	m^3/s
2	Salinity	0.01	psu
3	Temperature	25	°C
4	Oxygen	4	mg/L
5	Nitrite	0.04	mg/L

Table 3: Tidal Generation Constant Model

Constituent	Amplitude	Phase
M2	0.533325	-76.7706
S2	0.410785	-26.6992
K1	0.20178	150.2
K2	0.120774	-24.1747
N2	0.0771338	-84.739
2N2	0.0140409	-98.2157
O1	0.152388	127.784
Q1	0.066478	145.672
P1	0.0361863	118.223
M4	0	0
Mf	0.012547	12.7545
Mm	0.00753131	9.2493
Mtm	0.00214811	14.2702
MSqm	0.000306124	13.5703

3. RESULTS AND DISCUSSION

We have examined how tidal fluctuations influence key water quality parameters in our research location. Through continuous real-time monitoring for several weeks, detailed data related to ecological relevance and direct impact on aquaculture operations were collected on water level, dissolved oxygen, pH, salinity, temperature, nitrite, and electrical conductivity (**Fig. 3**). Autocorrelation and scatter plot analyses are presented in **Fig. 4** and **Fig. 5**, summary of statistical analyses is presented in

Table **4**:

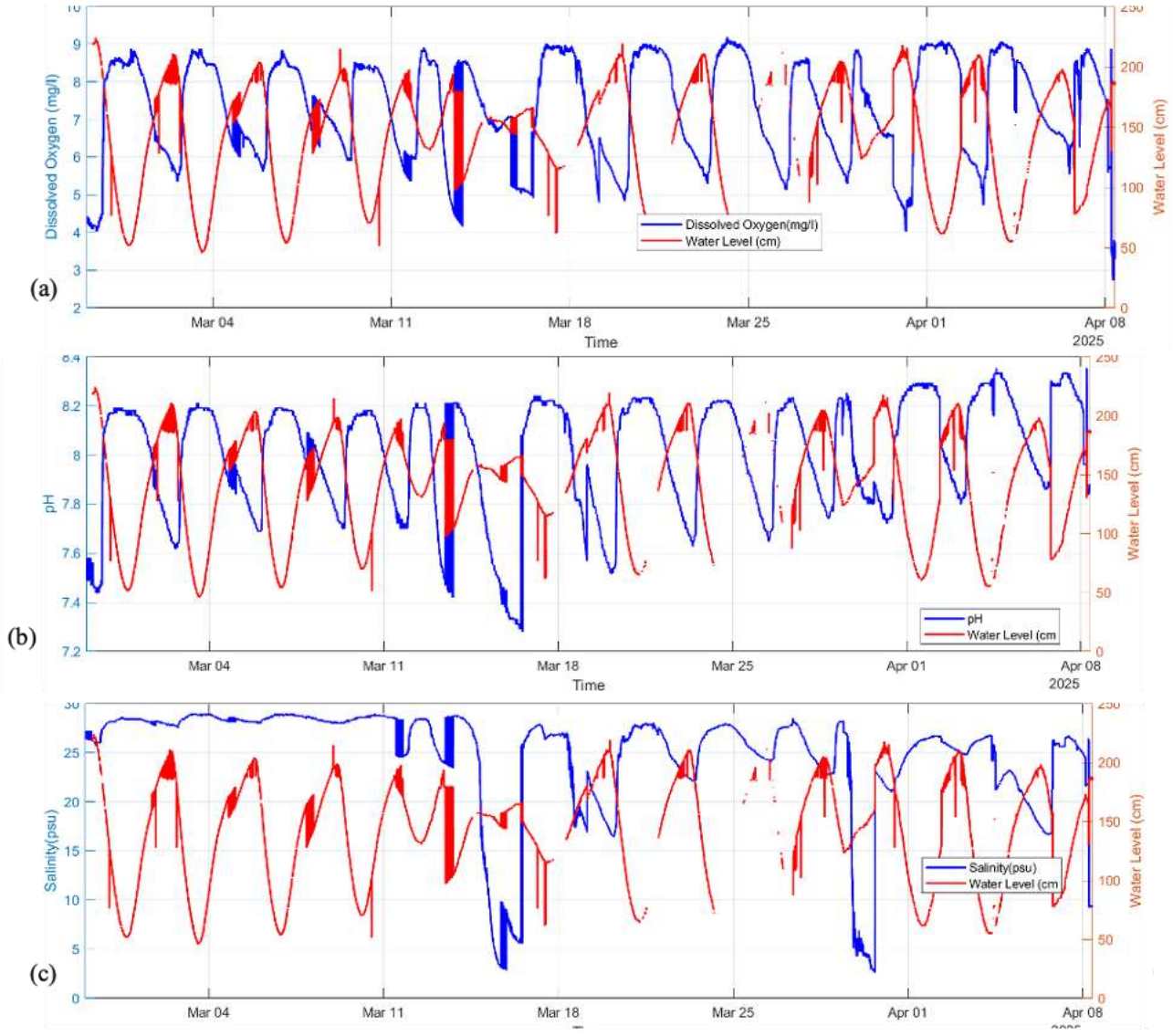

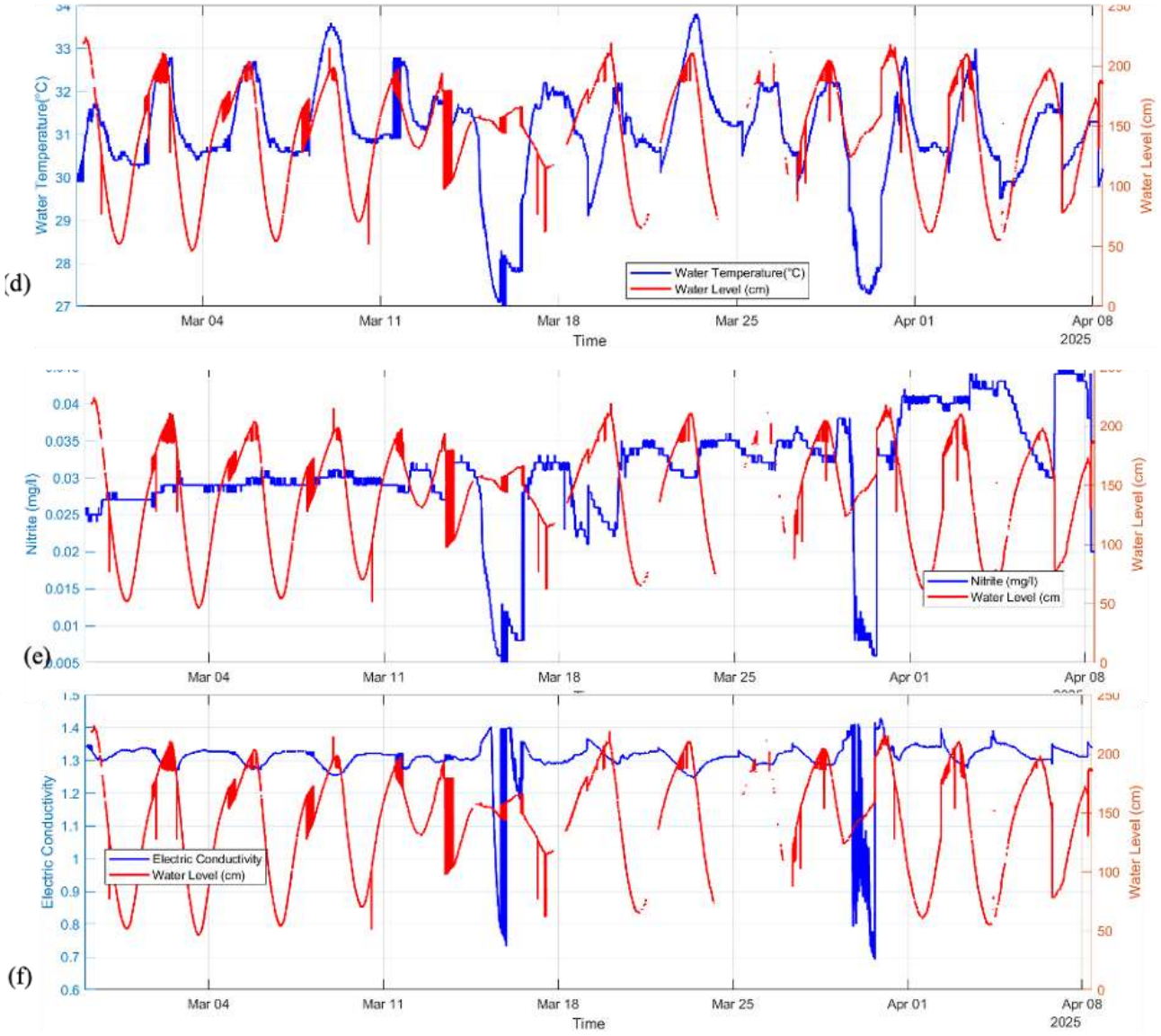

Fig. 3*:* Temporal dynamics of (a) dissolved oxygen; (b) pH; (c) salinity; (d) temperature; (e) nitrite; (f) EC against water levels observed from March to April 2025.

ACF and PCF analyses revealed strong serial dependence across all measured parameters (**Fig. 4**). The ACF exhibited slow, gradually decaying correlations, particularly for DO, pH, salinity, temperature, and nitrite, indicating that these variables changed progressively through time rather than randomly from one minute to the next. In contrast, water level displayed a clear cyclic pattern consistent with the semidiurnal tidal cycle (**Fig. 4**a).

The lag-1 autocorrelation coefficients (r_1) ranged from 0.77 for EC to above 0.98 for temperature and nitrite (

Table 4). Such high r1 values confirmed that successive 1-minute observations were not statistically independent, which would artificially inflate the degrees of freedom in uncorrected correlation tests. The PCAF plots further demonstrated that most of the temporal dependence could be explained by 1 to 2 preceding time steps, supporting the use of lag-1 coefficients to estimate N_eff.

To correct for this temporal autocorrelation, we applied the Pyper and Peterman adjustment based on the observed r1 of each variable (Pyper and Peterman, 1998). The resulting N_eff were substantially smaller than the raw sample size (9537), typically ranging between 680 and 1800 depending on each variable's persistence, which allowed more realistic significance testing of tidal relationship.

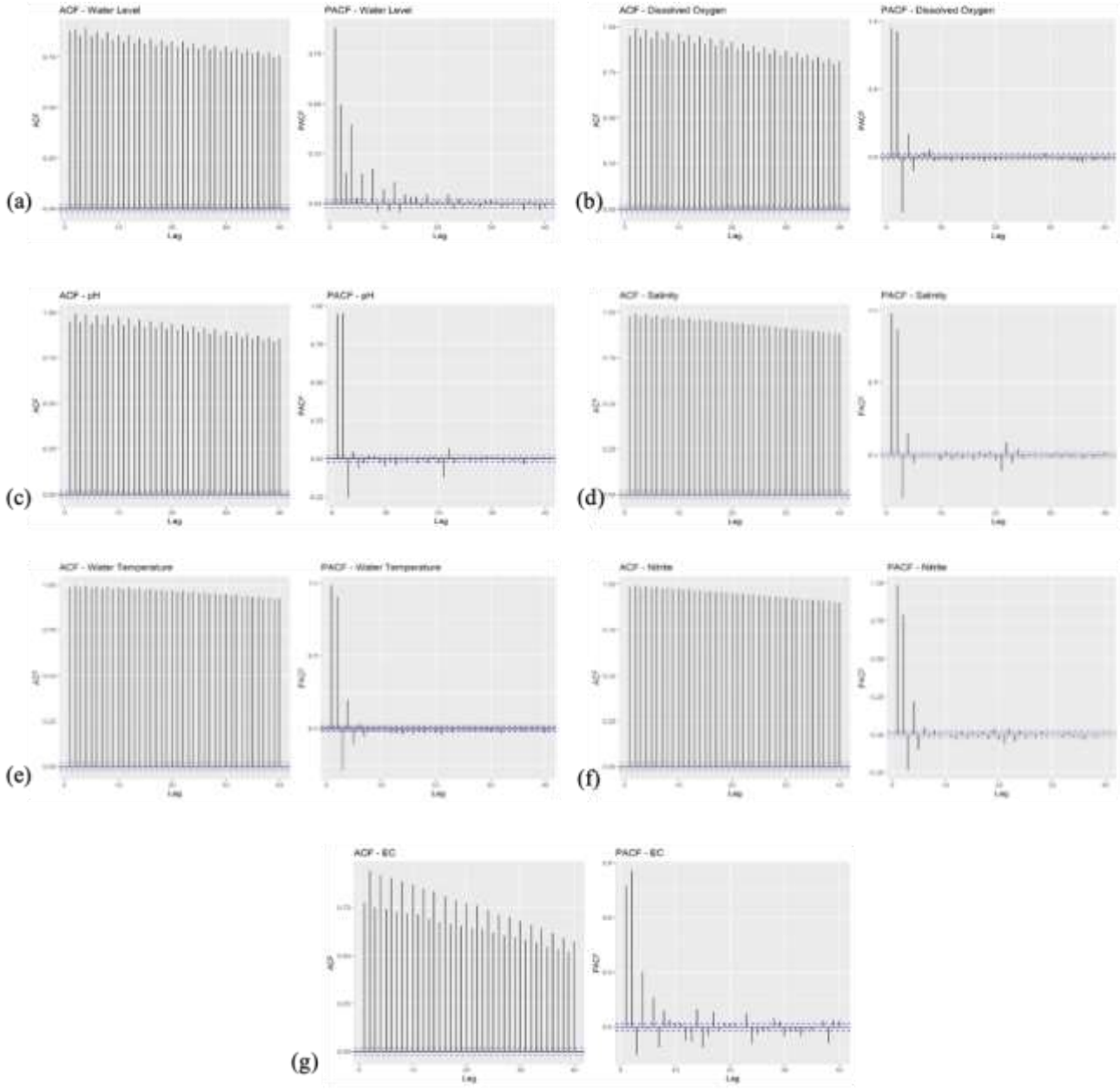

Fig. 4*:* Autocorrelation Function (ACF) and Partial Autocorrelation Function (PACF) analysis of (a) water level, (b) DO, (c) pH, (d) salinity, (e) temperature, (f) nitrite, and (g) EC.

Table 4: Pearson (linear) and Spearman (rank) correlations between tidal height (water level) and six water-quality variables (N complete = 9537)

Parameter	r_1 level	r_1 var	N_eff	Pearson *r*	Spearman ρ	Direction	Strength (rank)
DO	0.903	0.942	769	–0.663 (*p* < *0.0001*)	–0.764 (*p* < *0.0001*)		
pH	0.903	0.9393	783	–0.575 (*p* < *0.0001*)	–0.700 (*p* < *0.0001*)		
Salinity	0.903	0.9784	589	–0.274 (*p* < *0.0001*)	–0.385 (*p* < *0.0001*)		
Temperature	0.903	0.9846	560	+0.148 (*p* < *0.0001*)	+0.286 (*p* < *0.0001)*		
Nitrite	0.903	0.9852	557	–0.226 (*p* < *0.0001*)	–0.280 (*p* < *0.0001*)		
EC	0.903	0.7727	1698	–0.088 (*p* < *0.0001)*	–0.260 (*p* < *0.0001)*		

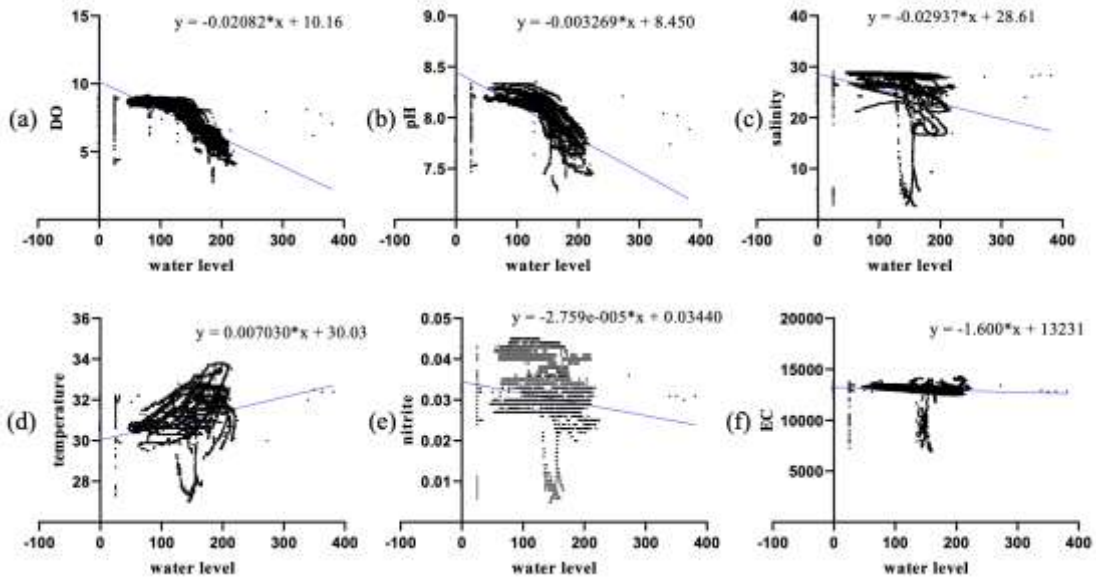

Fig. 5*:* Scatter plot between water level and (a) dissolved oxygen, (b) pH, (c) salinity, (d) temperature, (e) nitrite, and (f) EC.

3.1. Real-time effect of tidal changes on water quality

3.1.1. Water level

The water level sensor used in this study works by measuring hydrostatic pressure, which tells how high the water column is above the sensor. The pressure on the sensor changes as the water level changes with the tides. Then, this pressure is turned into an electrical signal, which is adjusted and turned into a reading of the water level

in centimeters. The sensor was able to accurately record the semidiurnal tidal cycle, which showed that water levels rose and fell about twice a day. As seen in **Fig. 3**a – 3f, the highest point is over 200 cm during high tide, and the lowest point is about 30 cm during low tide. High-resolution time series data obtained from sensors demonstrates its sensitivity and stability, making it crucial for monitoring changes in environments like mangrove estuaries, where rapid changes can impact water quality.

3.1.2. Dissolved Oxygen (DO)

The amount of DO in the mangrove area fluctuated with the tides, ranging from 5.6 to 7.8 mg/L (***Fig. 3***a). Higher concentrations were consistently recorded during low tide, suggesting enhanced oxygenation from freshwater inflows and turbulence. During high tide, seawater enters and becomes warmer and calmer, reducing its capacity to dissolve oxygen, particularly since seawater carries less oxygen than cooler, oxygen-rich upland freshwater.

Statistical analysis confirmed this pattern, revealing a strong negative correlation between water level and DO. Pearson correlation showed a strong negative correlation ($r = –0.663$), and Spearman confirmed this with an even stronger correlation($\rho = –0.764$). This pattern is visually evident in **Fig.** *5*a, where DO levels are higher during low tide. The tight clustering of data points along a downward curve reinforces the strength and consistency of this inverse relationship. Previous studies reported that DO levels below 5 mg/L are stressful to shrimp/fish (Patkaew et al., 2024). In contrast, our data showed that DO during low tide was consistently >6 mg/L, thereby supporting its suitability for water intake timing.

In addition to hydrodynamic mixing, biological processes also influence DO variability during the tidal cycle. Light penetration and water depth fluctuate with tides, which in turn affect photosynthetic activity by organisms such as phytoplankton and microalgae, as well as respiration by bacteria (Magni and Montani, 2004). Furthermore, DO levels have been found to correlate positively with chlorophyll-a concentrations and are subject to semi-diurnal tidal rhythms that influence oxygen dynamics and overall water quality in tidal creeks (MacPherson, Cahoon and Mallin, 2007).

Overall, our findings suggest that DO concentrations peak during low tide, when turbulence and freshwater inflows enhance aeration. These results strongly support the recommendation that pond water intake should occur during or shortly after low tide, when DO is at its most favorable level for aquaculture.

3.1.3. pH

The changes in pH levels in relation to tidal fluctuations are presented in **Fig.** 3b. The pH showed moderate fluctuations, typically ranging from 7.6 during high tide to 8.2 at low tide, with slightly higher values recorded when the water level was low. This decrease in pH during high tide is likely due to the buffering capacity of seawater, which tends to be more acidic compared to freshwater sources. In contrast, lower water levels allow greater influence from riverine and land-based inputs, which are generally more alkaline due to surrounding catchment characteristics.

Statistical analysis confirmed this pattern, with both Pearson (r = –0.575) and Spearman (ρ = –0.7) showing a strong negative relationship with water level (

Table 4). This relationship is also clearly reflected in **Fig.** 5b, where data points show a distinct downward slope. The mixing of seawater and freshwater during tidal changes leads to observable pH oscillations, with a phase lag behind tidal fluctuations. Moreover, biological activity such as aerobic respiration by aquatic organisms consumes DO and releases CO_2, which forms carbonic acid, thereby lowering the pH (Liu, Jiao and Liang, 2018). Additionally, local geological formations, vegetation types, and land use activities influence baseline alkalinity or acidity in the system (Omarjee et al., 2021). A study in Vietnam reported that mangrove stand age also significantly influenced pond pH, where older stands tended to slightly decrease pH due to organic matter decomposition and sulfide oxidation, but values remained within the optimal range for shrimp culture (Ngo et al., 2022).

Fluctuations in pH can have significant implications for aquaculture systems, as levels outside the optimal range may induce stress in cultured species and alter nutrient bioavailability, particularly for key compounds like ammonia and phosphate (Boyd, Tucker and Viriyatum, 2011). From our study, the consistent and predictable pattern of pH in response to tides makes it a reliable indicator of tidal influence, and a critical parameter to monitor for water quality management on mangrove-connected aquaculture zones

3.1.4. Salinity

Salinity data showed one of the clearest and most consistent responses to tidal changes throughout the monitoring period (**Fig.** 3c). Values ranged between 18 and 30 PSU, increasing noticeably during high tide as seawater intruded into the mangrove area and decreasing during low tide when freshwater from upstream sources became more dominant. This pattern closely aligns with expected estuarine mixing dynamics typically observed in coastal mangrove environments, where the balance between freshwater inflow and tidal intrusion controls the salinity gradient.

Pearson's correlation was r = –0.274, suggesting a moderate linear relationship, while Spearman's rank correlation (ρ = –0.385) indicated a stronger and more consistent monotonic trend. Although not perfectly linear, the pattern was reliably present across the data set. The increase in salinity during high tide and its dilution during low tide, as previously reported, support our data (Atekwana et al., 2022; S. and N. Z, 2024).

For aquaculture practitioners, understanding and anticipating these salinity shifts is essential. Drawing water into ponds during periods of extremely high or low salinity can disrupt the osmotic balance of aquatic species, which may lead to stress, slower growth, or even mortality. Salinity outside optimal ranges can impair the physiological performance of cultured species and reduce survival rates (Liang et al., 2023). Therefore, timing water intake in alignment with natural tidal rhythms is a fundamental aspect of sustainable and adaptive pond management in an estuarine environment.

3.1.5. Temperature

As shown in **Fig.** 3g, water temperature in the mangrove area ranged from 27°C and 33°C, fluctuating within a relatively narrow yet ecologically meaningful range. A slight increase in temperature was consistently observed during high tide, likely due to the intrusion of sun-warmed seawater from offshore areas. In contrast, cooler temperatures recorded during low tide may reflect the influence of freshwater from upstream regions or rainfall events.

Statistically, while the Pearson correlation between temperature and water level was significant but weak ($r = 0.148$, $p < 0.001$), the Spearman correlation was weak-moderate ($\rho = 0.286$, $p < 0.001$), suggesting a consistent monotonic trend, where warmer temperatures tend to coincide with higher water levels, as further visualized in **Fig.** 5d.

Although these temperature shifts may seem subtle, they are not without consequence. Even minor thermal changes can influence DO solubility, alter metabolic rates, and affect the stress tolerance of aquaculture species. In sensitive environments such as mangroves, temperature plays a crucial role in determining the health and distribution of both flora and fauna. For instance, studies from Florida's Gulf Coast have shown that rising temperatures are linked to the poleward expansion of mangrove forests, with increases in canopy height and coverage as minimum temperatures rise (Kang, Kaplan and Osland, 2024). Similarly, in the Kali Estuary, fluctuations in water temperature are closely associated with changes in salinity, pH, and nutrient concentrations, underscoring the interdependence of hydrographic parameters (Xie et al., 2014). Given its subtle but influential role in the aquatic environment, water temperature remains an important parameter to monitor, particularly with tidal dynamics and overall water quality stability in mangrove-connected aquaculture systems.

3.1.6. Nitrite

Nitrite concentrations remained relatively low throughout the monitoring period, typically between 0.015 and 0.035 mg/L, yet showed a predictable increase several hours after low tide (**Fig.** 3e). This delayed rise is most likely driven by sediment resuspension and intensified microbial activity, as the receding tide may expose and mobilize organic matter trapped in the benthic substrate. Although nitrite levels exhibited only a weak relationship with water level, with both Pearson and Spearman correlations (see

Table 4:), the scatter plot revealed a broad dispersion of data points, with only a slight tendency for nitrite to increase following low tide (**Fig.** 5e).

Our pattern aligns with findings from other recent studies. DO fluctuations and nitrite accumulation driven by tidal mixing, organic-matter decomposition, and sediment fluxes have also been reported in other tropical estuarine and mangrove systems. For example, tidal mixing shapes how mangroves exchange nutrients with the estuary by influencing oxygen levels and redox conditions, which in turn govern the transformation between ammonium, nitrite, and nitrate and affect the system's overall nutrient balance (Wang et al., 2021). Furthermore, sediment resuspension during tidal cycles significantly enhances nutrient release, including nitrites, into the water

column in estuarine systems (Rios-Yunes et al., 2023). Similarly, another study observed that nitrite-reducing and nitrifying bacteria become highly active during the transition between exposed and submerged conditions, leading to an episodic pulse of nitrite in intertidal sediments (Chen et al., 2021).

Although nitrite concentrations in this study remained within safe limits for aquaculture, the consistent post-ebb increase emphasizes a potential risk if water is drawn into ponds during this window. Therefore, while tidal height alone may not strongly predict nitrite behavior, the timing of microbial processes and sediment dynamics demonstrates the need for independent and frequent nitrite monitoring. Avoiding water intake shortly after low tide may help reduce nitrite accumulation.

3.1.7. Electric conductivity (EC)

Unlike other water quality parameters, EC showed little to no consistent connection to tidal fluctuations (**Fig.** 3f and 4f). EC is fundamentally linked to the concentration of ions within the water, with salinity, largely determined by the sodium chloride (Rameshkumar et al., 2019). In typical estuarine systems, tidal exchanges introduce predictable salinity gradients, leading to a positive correlation between water level, salinity, and EC (Rusydi, 2018). However, our data unveiled a more intricate scenario. The scatter plot displays a diffuse pattern, lacking any clear trend between water level and EC. This visual pattern is consistent with the statistical data ($r = -0.088$ and $\rho = -0.26$), suggesting an indirect association. Furthermore, it suggests that the ionic composition of the water at our study site is subject to influences beyond simple tidal-driven salinity fluctuations.

Indeed, natural aquatic systems rarely conform to simplified models. It is influenced by a combination of freshwater inflow, surface runoff, and possible anthropogenic discharges, all of which can significantly modify the ionic composition of water.

3.2. 3D tidal and water quality model simulation

In addition to field monitoring and statistical analysis, we used OpenFlow Flood 3D simulation to better understand how tidal movements behave within the seawater, mangrove, and aquaculture zone (Sabhan *et al.*, 2019). By feeding the model with actual topography, bathymetry, and real-time tidal data from the site, we were able to simulate how water moves through the system during different tidal phases and affects water quality.

The model results show the spatial distribution of water quality parameters from the river, which is the raw water source for the pond in Tanah Mea village, to the open sea in the Makassar Strait. The results of the sample point (119.617423, -0.824804) at the river mouth show the relationship between tides and water quality parameters (**Fig. 6**). The type of tide at the research location is a mixed tide leaning towards a semi-diurnal with a Formzhal number of 0.375.

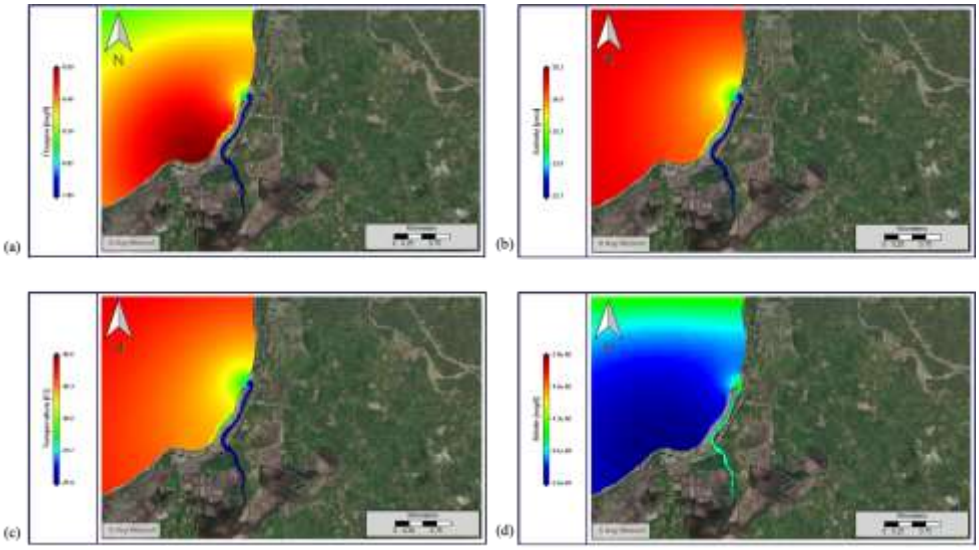

Fig. 6 Simulation of tidal fluctuations affecting (a) dissolved oxygen, (b) salinity, (c) temperature, and (d) nitrite.

The simulation of DO during high tide shows a clear difference in oxygen levels from the river to the sea (**Fig. 6**a). In the upstream river, DO levels are relatively low (7.80-8.00 mg/L), most likely due to organic waste, domestic discharge, and nearby pond activities. This input contributes to increased biochemical oxygen demand, depleting the availability of oxygen for aquatic life (Cheng et al., 2024). Even when the tide brings seawater into the estuary, the DO levels do not improve much. This suggests that the incoming tidal water already mixes with poorer quality river water before it gets any closer to the ponds. In contrast, coastal and open sea regions show a rise in DO, visualized by yellow-red tones, driven by cleaner waters, stronger circulation, and wave-induced aeration, all of which enhance the continuous replenishment of oxygen in the water column (Zhang et al., 2022).

The salinity model reveals a clear gradient from the river to the sea (**Fig. 6**b). In the upstream river, salinity is low (22.3-23.8 PSU), reflecting the strong influence of freshwater. As water moves toward the river mouth, salinity rises slightly (23.8-25.3 PSU), indicating an active mixing zone between freshwater and incoming sea-water (Monismith, 2017). During high tide, saltier seawater with a salinity of >26.8 PSU reaches the coast and partly enters the estuary with limited intrusion, resulting in domination of a moderate salinity level in the pond area (Guo *et al.*, 2019).

The model of temperature distribution at high tide shows an increasing pattern from the upstream of the river to the open sea (**Fig. *6***c). In the upstream estuary, the temperature is relatively low (29.4–29.7°C) due to the influence of fresh water and vegetation, similar to the previously reported study (Shen *et al.*, 2022). Entering the estuary, the temperature rises to 29.7–30.0°C due to the mixing of freshwater and seawater. In the open sea, temperatures increase significantly (30.3–30.6°C) due to exposure to sunlight and the shallowness of the waters, which allows rapid heating. This pattern shows a consistent temperature gradation from land to sea, confirming that tides, waves, and river inflow in our study play critical roles in determining temperature variations of the local estuarine, similar to the study in the San Francisco Estuary (Bashevkin and Mahardja, 2022).

The nitrite distribution model reflects a clear tidal-driven pattern (**Fig. 6**d). The elevated concentrations originated from southern river inflows, likely influenced by agricultural and aquaculture runoff. As this water reaches the estuary, nitrite levels remain relatively high (0.013–0.016 mg/L), even during high tide, when seawater enters inland canals and serves as raw water for nearby ponds. However, the seawater is already mixed with nitrite-rich river water, posing a contamination risk (Suratman *et al.*, 2018). Further seaward, nitrite concentrations decline significantly (0.0055–0.009 mg/L), diluted by a larger volume of open seawater.

Fig. 7 shows simulation models of tidal fluctuations against selected water quality parameters. Salinity fluctuates synchronously with the tides (**Fig. 7**b). When the tide is high, the salinity increases, signaling the entry of salt-rich seawater masses. Salinity, on the other hand, drops as the water recedes because fresh water from the river predominates. The surface temperature of the water also fluctuates, but with a weaker correlation to tides (**Fig. 7**c). There is a tendency for temperatures to rise at high tide, likely due to warmer seawater entering coastal areas. However, daily factors like solar radiation also influence temperature fluctuations. Nitrite levels tend to decrease at high tide and increase at low tide. This means that when seawater enters, the nitrite concentration decreases due to the dilution effect. On the other hand, at low tide, nitrite-rich river water from domestic and agricultural waste is more dominant. DO exhibits a pattern that follows the ups and downs of the tides (**Fig. 7**a). Generally, at high tides, DO levels increase, as seawater carries oxygen higher than the open sea. At low tide, the DO decreases because the river water entering the system has lower oxygen levels due to organic loads.

These observed patterns confirm the importance of multivariate predictive analysis in forecasting changes in tidal-water quality parameters, particularly due to the unpredictable nature of climate change (Khosravi *et al.*, 2023)

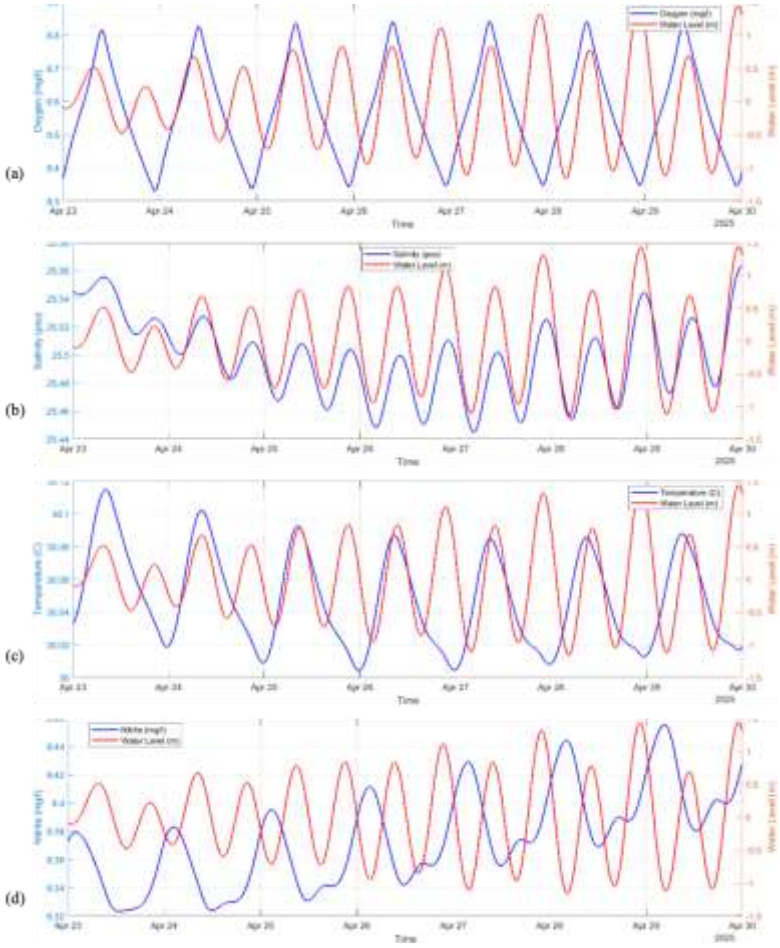

Fig. 7 simulation models of tidal fluctuations against (a) DO, (b) salinity, (c) temperature, (d) nitrite.

To complement our findings obtained from WQMS-based monitoring and statistical analysis with those derived from 3D hydrodynamic simulation, we did a comparative summary. While each method offers a unique perspective, their integration allows for a more holistic interpretation of water quality dynamics under tidal influence. Table 5 below presents a synthesis of both approaches, highlighting areas of alignment and divergence and offering practical insights for aquaculture water management in the Tanah Mea region.

Table 5: Comparison of WQMS monitoring vs. 3D simulation results

Parameter	WQMS & statistical analysis	3D simulation mode	Aquaculture recommendation
DO	Ranged from 5.6–7.8 mg/L; consistently higher during low tide. Strong negative correlation ($r = -0.663$; $\rho = -0.764$).	Spatially lower upstream (7.80–8.00 mg/L), increases gradually toward the sea (up to 8.68 mg/L).	Draw water during or after low tide to ensure higher oxygen levels and better pond aeration.

pH	Slightly fluctuated between 7.6 and 8.2; lower during high tide due to seawater buffering. Strong negative correlation.	Not spatially simulated.	Monitor pH routinely to maintain the optimal range for nutrient availability and species tolerance.
Salinity	Ranged from 18 to 30 PSU; increased during high tide and decreased during low tide. Moderate negative correlation.	Low upstream (22.3–23.8 PSU), transitional in estuary (23.8–25.3 PSU), and highest near sea (>26.8 PSU).	Avoid water intake during extreme salinity levels; regulate timing based on tidal cycle.
Temperature	Ranged from 27°C to 33°C; slightly warmer during high tide. Weak correlation (r = 0.148), but clear Spearman trend.	Cooler in rivers (29.4°C), warmer in the sea (30.6°C); reflects solar exposure and depth.	Consider temperature trends, especially for species sensitive to thermal shifts.
Nitrite	Generally low (0.015–0.035 mg/L); rises after low tide, possibly from sediment resuspension. Weak correlation (r ≈ –0.226).	High in rivers (0.016–0.020 mg/L), diluted downstream; lowest near open sea (<0.009 mg/L).	Avoid water intake shortly after low tide to reduce risk of nitrite buildup in ponds.
EC	Weak correlation with tides (r = –0.088); pattern inconsistent. Possibly affected by rainfall or runoff.	Not explicitly modeled spatially.	Use EC only in combination with pH and salinity to assess overall water chemistry.

The timing of water exchange is a critical factor in shrimp farming, as mangrove estuaries undergo tidal and biogeochemical fluctuations that influence water quality. For example, a study in a tidal mangrove creek in Australia reported that shrimp farm effluent increased nutrient levels in the receiving creek, and stable isotope evidence showed that these impacts extended into the intake creek, highlighting potential risks for pond water replenishment (Costanzo, O'Donohue, and Dennison, 2004). Furthermore, mangroves regulate water intake by excluding salts at the root level, maintaining sources when available, thereby ensuring survival and productivity under saline conditions (Reef and Lovelock, 2015). It is therefore recommended that water intake be scheduled during low tide or after effluent dilution, when water quality is more stable, dissolved oxygen concentrations are consistently higher, and conditions are more favorable for shrimp culture.

The integration of real-time field monitoring using WQMS and spatial simulation through OpenFlows Flood provides a comprehensive understanding of the tidal influences on water quality in Tanah Mea enstuarine mangrove area. The 3D simulation complements the high-resolution temporal data provided by the WQMS system by visualizing the spatial distribution of parameters such as temperature, nitrite, salinity, and DO during tidal movements. However, the observed DO patterns from the WQMS did not fully align with the modeled outputs, likely due to the depth-averaged assumption and omission of fine-scale local processes. During high tides, the incoming water may carry higher organic matter loads, stimulating aerobic microbial activity that increases oxygen consumption. In addition, elevated temperature or salinity during high tide may further reduce DO solubility. Local stratification

may also occur, as the WQMS sensor is near the estuary bottom, whereas the model represents depth-averaged values. These local and physical factors can explain the apparent discrepancies between the observed and modeled DO trends. Despite these differences, both datasets consistently captured key tidal patterns, which underscoring the complementary value of integrating field observation and hydrodynamic modeling. This dual approach improves our understanding of site-specific processes and supports practical recommendations for pond water management, particularly water intake during low tide phases when DO tends to be higher and nitrite concentrations lower.

4. CONCLUSIONS

This study demonstrated that tidal fluctuations significantly influence water quality dynamics in the Tanah Mea mangrove–estuarine system of Central Sulawesi. By integrating real-time monitoring using Water Quality Monitoring System (WQMS) sensors with spatial simulations in OpenFlows Flood, we identified clear and ecologically meaningful responses of temperature, dissolved oxygen (DO), pH, salinity, and nitrite to tidal changes. DO and pH tended to be higher during low tide, while salinity and temperature increased with high tide; however, the modeled DO patterns did not fully align with field observations, likely due to the depth-averaged model assumption and unrepresented local processes such as benthic oxygen demand, stratification, and organic matter inputs during flood tides. Despite these discrepancies, both datasets consistently revealed key tidal patterns and spatial gradients across the estuary, highlighting the complementary value of combining empirical and modeling approaches. This integration enhances understanding of short-term and spatially variable water quality changes that are critical for aquaculture management—particularly for determining optimal water intake timing in shrimp and fish ponds—and provides a replicable framework for sustainable estuarine aquaculture management in other tropical coastal systems.

5. PATENTS

Author Contributions: “Conceptualization, P.S. and S.S.; methodology, P.S., S.S., M.I. N.I.I; software, P.S., S.S.; validation, P.S. and N.I.I; writing—original draft preparation, P.S.; writing—review and editing, A.T.; visualization, S.S.; project administration, P.S.; funding acquisition, P.S. and A.T. All authors have read and agreed to the published version of the manuscript.”

Funding: This work received financial support from Indosat Ooredoo Hutchison and the DIPA Unggulan Universitas Tadulako under Grant Number 4620/UN28/HK.02/2025.

Acknowledgments: We would like to express our gratitude to Indosat Ooredoo Hutchison for providing WQMS tools, a real-time monitoring website, and CSR funding.

Conflicts of Interest: “The authors declare no conflicts of interest.” “The funders had no role in the design of the study; in the collection, analysis, or interpretation of data; in the writing of the manuscript; or in the decision to publish the results.”

REFERENCES

1. Abdelmoneim, Kimaita, H.N., Al Kalaany, C.M., Deredja, B., Dragonetti, G. and Khandra, R. 2025 IoT Sensing for Advanced Irrigation Management: A Systematic Review of Trends, Challenges, and Future Prospects, *Sensors*, 25(7), p. 2291. [DOI]

2. Atekwana, E.A. Ramatlapeng, G.J., Ali, H.N., Njilah, I.K. and Ndondo, G.R.N. 2022 Tide-salinity patterns reveal seawater-freshwater mixing behavior at a river mouth and tidal creeks in a tropical mangrove estuary, *Journal of African Earth Sciences*, 196, p. 104684. [DOI]

3. Bashevkin, S.M. and Mahardja, B. 2022 Seasonally variable relationships between surface water temperature and inflow in the upper San Francisco Estuary, *Limnology and Oceanography*, 67(3), pp. 684–702. [DOI]

4. Boyd, C.E., Tucker, C.S. and Viriyatum, R. 2011 Interpretation of pH, Acidity, and Alkalinity in Aquaculture and Fisheries, *North American Journal of Aquaculture*, 73(4), pp. 403–408. [DOI]

5. Chen, F. Zheng, Y., Hou, L., Niu, Y., Gao, D., An, Z., Zhou, J., Yin, G., Dong, H., Han, P., Liang, X. and Liu, M. 2021 Microbial abundance and activity of nitrite/nitrate-dependent anaerobic methane oxidizers in estuarine and intertidal wetlands: Heterogeneity and driving factors', *Water Research*, 190, p. 116737. [DOI]

6. Cheng, S., Meng, F., Wang, Y., Zhang, J. and Zhang, L. 2024 The potential linkage between sediment oxygen demand and microbes and its contribution to the dissolved oxygen depletion in the Gan River, *Frontiers in Microbiology*, 15, p. 1413447. [DOI]

7. Costanzo, S.D., O'Donohue, M.J. and Dennison, W.C. 2004 Assessing the influence and distribution of shrimp pond effluent in a tidal mangrove creek in north-east Australia, *Marine Pollution Bulletin*, 48(5–6), pp. 514–525. [DOI]

8. Essamlali, I., Nhaila, H. and El Khaili, M. 2024 Advances in machine learning and IoT for water quality monitoring: A comprehensive review, *Heliyon*, 10(6), p. e27920. [DOI]

9. Guo, Q., Huang, J., Zhou, Z. and Wang, J. 2019 Experiment and Numerical Simulation of Seawater Intrusion under the Influences of Tidal Fluctuation and Groundwater Exploitation in Coastal Multilayered Aquifers, *Geofluids*, 2019, pp. 1–17. [DOI]

10. Guo, Y., Liu, C., Ye, R. and Duan, Q. 2020 Advances on Water Quality Detection by UV-Vis Spectroscopy', *Applied Sciences*, 10(19), p. 6874. [DOI]

11. Kang, Y., Kaplan, D.A. and Osland, M.J. 2024 Linking temperature sensitivity of mangrove communities, populations and individuals across a tropical‐temperate transitional zone, *Journal of Ecology*, 112(6), pp. 1256–1274. [DOI]

12. Khosravi, M., Duti, B.M., Yazdan, M.M.S, Ghoochani, S., Nazemi, N. and Shabanian, H. 2023 Multivariate Multi-Step Long Short-Term Memory Neural Network for Simultaneous Stream-Water Variable Prediction', *Eng*, 4(3), pp. 1933–1950. [DOI]

13. Kusumaningtyas, M.A., Kepel, T.L., Solihuddin, T., Lubis, A.A., Putra, A.D.P., Sugiharto, U., Ati, R.N.A., Salim, H.L., Mustikasari, E., Heriati, A., Daulat, A., Sudirman, N., Suryono, D.D. and Rustam, A. 2022 Carbon sequestration potential in the rehabilitated mangroves in Indonesia , *Ecological Research*, 37(1), pp. 80–91. [DOI]

14. Lam, K.-L., Lam, Y.-H., Ng, A.Y.-S., So, K.K.-Y., Tam, N.F.-Y., Lee, F.W.-F. and Mo, W.-Y. 2023 The Impact of Anthropogenic Pollution on Tidal Water Quality in Mangrove Wetlands', *Journal of Marine Science and Engineering*, 11(12), p. 2374. [DOI]

15. Liang, D., Testa, J.M., Gurbisz, C. and Harris, L.A. 2023 A Spatiotemporal Synthesis of High-Resolution Salinity Data with Aquaculture Applications', in *I-GUIDE Forum 2023: Harnessing the Geospatial Data Revolution for Sustainability Solutions*. *I-GUIDE Forum*, Purdue University Library Publishhing. [DOI]

16. Liu, Y., Jiao, J.J. and Liang, W. 2018 Tidal Fluctuation Influenced Physicochemical Parameter Dynamics in Coastal Groundwater Mixing Zone, *Estuaries and Coasts*, 41(4), pp. 988–1001. [DOI]

17. MacPherson, T.A., Cahoon, L.B. and Mallin, M.A. 2007 Water column oxygen demand and sediment oxygen flux: patterns of oxygen depletion in tidal creeks, *Hydrobiologia*, 586(1), pp. 235–248. [DOI].

18. Magni, P. and Montani, S. 2004 Physical and Chemical Variability of Tidal Streams," in J.H. Lehr and J. Keeley (eds.) *Water Encyclopedia*. 1st ed. Wiley, pp. 128–133. [DOI]

19. Mitra, R. and Sikder, V. 2023 Impact ofbrackish water aquaculture and mangrove degradation on global carbon balance: a review, *The holistic approach to environment*, 13(2), pp. 76–82. [DOI]

20. Monismith, S. 2017 An integral model of unsteady salinity intrusion in estuaries, *Journal of Hydraulic Research*, 55(3), pp. 392–408. [DOI]

21. Ngo, T.T.D., Nguyen, T.C.T, Vo, T.T.P., Tran, L.K., Nguyen, T.H., Nguyen, D.T.N., Tran, D.D. and Dang, T.T.T. 2022 Factors affecting water quality and shrimp production in the mixed mangrove - shrimp systems in the Mekong Delta of Vietnam, *Aquaculture Research*, 53(2), pp. 497–517. [DOI]

22. Omarjee, A., Taljaard, S., Ramjukadh, C.-L. and Niekerk, L., 2021 pH variability in catchment flows to estuaries – A South African perspective, *Estuarine, Coastal and Shelf Science*, 262, p. 107605. [DOI].

23. Palit, K., Rath, S., Chatterjee, S. and Das, S. 2022 Microbial diversity and ecological interactions of microorganisms in the mangrove ecosystem: Threats, vulnerability, and adaptations, *Environmental Science and Pollution Research*, 29(22), pp. 32467–32512. [DOI]

24. Patkaew, S., Direkbusarakom, S., Hirono, I., Wuthisuthimethavee, S., Powtongsook, S. and Pooljun, C. 2024 Effect of supersaturated dissolved oxygen on growth-, survival-, and immune-related gene expression of Pacific white shrimp (Litopenaeus vannamei), *Veterinary World*, pp. 50–58. [DOI]

25. Pyper, B.J. and Peterman, R.M. 1998Comparison of methods to account for autocorrelation in correlation analyses of fish data," *Canadian Journal of Fisheries and Aquatic Sciences*, 55(9), pp. 2127–2140. [DOI]

26. Rahman Lokollo, F.F., Manuputty, G.T., Hukubun, R.D., Krisye, Maryono, Wawo, M. and Wardiatno, Y. 2024 A review on the biodiversity and conservation of mangrove ecosystems in Indonesia, *Biodiversity and Conservation*, 33(3), pp. 875–903. [DOI]

27. Rameshkumar, S., Radhakrishnan, K., Aanand, A. and Rajaram R. 2019 Influence of physicochemical water quality on aquatic macrophyte diversity in seasonal wetlands, *Applied Water Science*, 9(1), p. 12. [DOI].

28. Reef, R. and Lovelock, C.E. 2015 Regulation of water balance in mangroves, *Annals of Botany*, 115(3), pp. 385–395. [DOI]

29. Rios-Yunes, D., Grandjean, T., Primio, A., Tiano, J., Bouma, T.J., Oevelen, D. and Soetaert, K. 2023 Sediment resuspension enhances nutrient exchange in intertidal mudflats, *Frontiers in Marine Science*, 10, p. 1155386. [DOI]

30. Rusydi, A.F. 2018 Correlation between conductivity and total dissolved solid in various type of water: A review, *IOP Conference Series: Earth and Environmental Science*, 118, p. 012019. [DOI]

31. S., Nurhidayu. and N. Z, H. 2024 Tidal And Seasonal Effects on Water Quality in the Matang Mangrove Forest Reserve, Malaysia, *Modern Applied Science*, 18(1), p. 39. [DOI]

32. Sabhan, Koropitan, A.F., Purba, M. and Pranowo, W.S. 2019 3D Simulation Model of Tidal, Internal Mixing and Turbulent Kinetic Energy of Palu Bay, *Nature Environment and Pollution Technology*, 18(4), pp. 1083–1094 [Google Scholar].

33. Shen, H., Zhu, Y., He, Z., Li, L. and Lou, Y. 2022 Impacts of River Discharge on the Sea Temperature in Changjiang Estuary and Its Adjacent Sea, *Journal of Marine Science and Engineering*, 10(3), p. 343. [DOI].

34. Singh, A.R., Thirumurugan, V. and Prabakaran, N. 2024 Monitoring the Mangrove Colonization on the Uplifted Reef Beds in the North Andaman Island, India, *Ocean Science Journal*, 59(3), p. 32. [DOI].

35. Singh, J.K. 2020 Structural characteristics of mangrove forest in different coastal habitats of Gulf of Khambhat arid region of Gujarat, west coast of India, *Heliyon*, 6(8), p. e04685. [DOI]

36. Singh, Y. and Walingo, T. 2024 Smart Water Quality Monitoring with IoT Wireless Sensor Networks, *Sensors*, 24(9), p. 2871. [DOI]

37. Srivastava, S., Vaddadi, S. and Sadistap, S. 2018 Smartphone-based System for water quality analysis, *Applied Water Science*, 8(5), p. 130. [DOI]

38. Suharno and Saraswati, E. 2020 The Identification of Mangrove Ecosystem Services for Decision Making, *SHS Web of Conferences*. Edited by W.R. Adawiyah et al., 86, p. 01019. [DOI]

39. Suratman, S., Aziz, A.A., Tahir, N.M. and Lee, L.H. 2018 Distribution and Behaviour of Nitrogen Compounds in the Surface Water of the Sungai Terengganu Estuary, Southern Waters of South China Sea, Malaysia, *Sains Malaysiana*, 47(4), pp. 651–659. [DOI]

40. Wang, F. Cheng, P., Chen, N and Kuo, Y-M 2021 Tidal driven nutrient exchange between mangroves and estuary reveals a dynamic source-sink pattern, *Chemosphere*, 270, p. 128665. [DOI]

41. Wang, Y., Rajib, S.M.S.M., Collins, C. and Grieve, B. 2018 Low-Cost Turbidity Sensor for Low-Power Wireless Monitoring of Fresh-Water Courses, *IEEE Sensors Journal*, 18(11), pp. 4689–4696. [DOI].

42. Wessa, P. 2025 Free Statistics Software. *Office for Research Development and Education*. [URL].

43. Xie, X., Zhang, M.-Q., Zhao, B. and Guo, H.-Q. 2014 Dependence of coastal wetland ecosystem respiration on temperature and tides: a temporal perspective, *Biogeosciences*, 11(3), pp. 539–545. [DOI].

44. Zhang, F., Zhi, X., Zhao, S., Arvola, L., Huotari, J. and Hao, R. 2022 Equilibrium simulation and driving factors of dissolved oxygen in a shallow eutrophic Inner Mongolian lake (UL) during open-water period, *Water Supply*, 22(6), pp. 6013–6031.[DOI]